Supporting Information for

Ultra-thin Two-dimensional Molecular Crystals Grown on a Liquid Surface for High-Performance Phototransistors

Shuyuan Yang,‡[a] Yu Zhang,‡[a] Ying Wang,[a] Jiarong Yao,[a] Lijuan Zhang,[a] Xiaochen Ren,[a] Xiaozeng Li,[a] Shengbin Lei,[a] Xiaotao Zhang,[a] Fangxu Yang,*[a] Rongjin Li *[a] and Wenping Hu [ab]

[a.] Tianjin Key Laboratory of Molecular Optoelectronic Sciences, Department of Chemistry, School of Science, Tianjin University & Collaborative Innovation Center of Chemical Science and Engineering (Tianjin), Tianjin 300072, China.

[b.] Joint School of National University of Singapore and Tianjin University, International Campus of Tianjin University, Binhai New City, Fuzhou 350207, China.

* Email: yangfangxu@tju.edu.cn, lirj@tju.edu.cn

Materials: C_{10}-DNTT was purchased from Lumtec. All materials were used without purification.

Substrate preparation: SiO_2 (300 nm)/Si wafers were cleaned by sonication in deionized water, acetone, and isopropanol for 10 min successively. Then, the SiO_2/Si wafers were treated by oxygen plasma at 80 W for 10 min followed by modification with octadecyltrichlorosilane (OTS) by a vapor phase method. The OTS-modified wafers were sequentially cleaned by chloroform, acetone, and isopropanol for 10 min, and dried with nitrogen.

Characterization: Optical and cross-polarized optical microscope images were obtained with a Nikon ECLIPSE Ci-POL polarized optical microscope. TEM and SAED measurements were performed on a Tecnai G2 F20 S-TWIN. XRD measurements were carried out in reflection mode at 45 kV and 200 mA with monochromatic Cu Kα radiation utilizing a Rigaku Smartlab diffractometer. UV–vis absorption spectrum of 2DMCs of C_{10}-DNTT was measured with a SHZMADZU UV-3600 Plus spectrophotometer. Intelligent mode AFM was

performed using a Bruker Dimension Icon. OFET and OPT characteristics were measured using a micromanipulator 6150 probe station connected to a Keithley 4200-SCS. All measurements were carried out in ambient air at room temperature. The photoresponse characteristics were evaluated by a laser generator with tunable power density. The laser power density was measured in-situ by a light intensity meter PM100D.

Figures of Merit of OPTs: The key figures of merit such as external quantum efficiency (EQE), *R*, *P*, and D^* are critical parameters for evaluating the optical response performance of OPTs. *P* is calculated by the following equation $P = (I_{light} - I_{dark}) / I_{dark}$, where I_{light} and I_{dark} are the drain-source current under illumination and in dark conditions, respectively. *R* is given by $R = (I_{light} - I_{dark}) / P_{in}$, where P_{in} is the incident light power. Meanwhile, EQE is decided by *R*, according to $\mathrm{EQE} = Rhc / \lambda e$, where *c* is the speed of light, *h* is the Planck constant, λ is the wavelength of the incident light, *e* is the unit charge. D^* is given by $D^* = RS^{1/2} / (2eI_{dark})^{1/2}$ when the shot noise of dark current dominates noise current, where *S* is the area of channel.

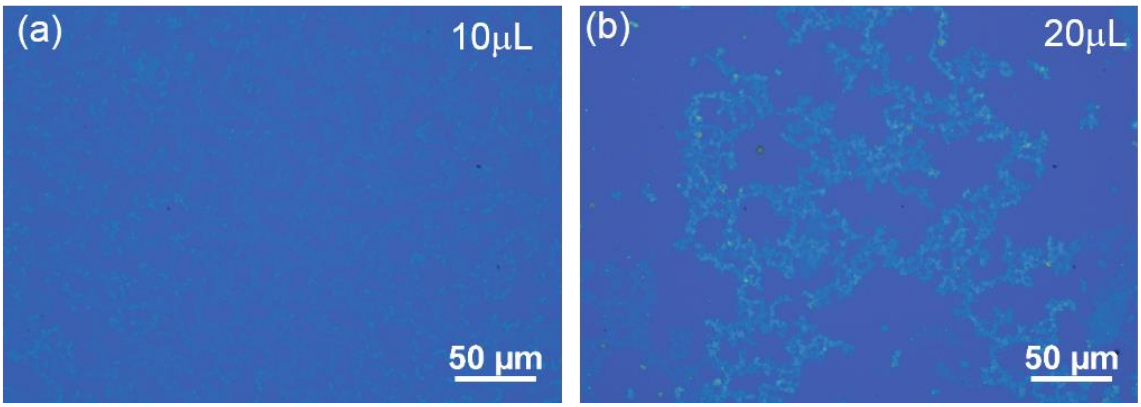

Figure S1. (a-b) Optical microscopy images of C_{10}-DNTT crystals grown with small volumes of C_{10}-DNTT solution.

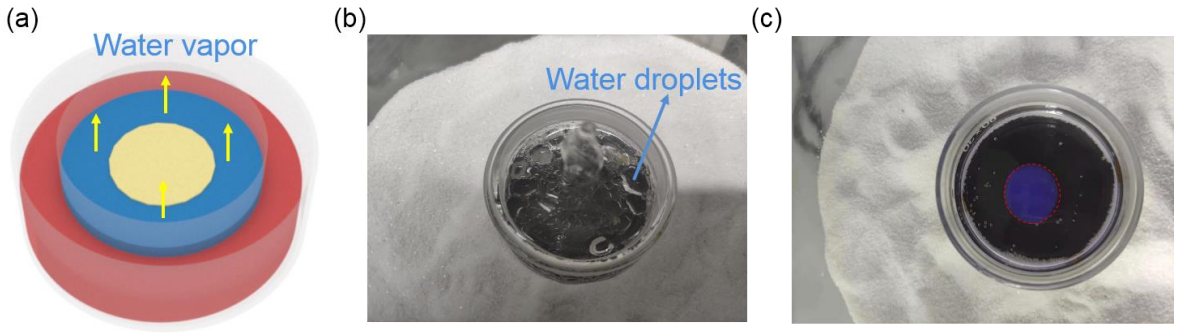

Figure S2. (a) A schematic diagram showing the evaporation of water vapor at high temperature during crystal growth on water surface. (b) Water droplets was found on the cap after crystal growth. (c) Spreading of C_{10}-DNTT on the surface of glycerol at a high growth temperature of 75°C. The solution spreads out into a continuous film.

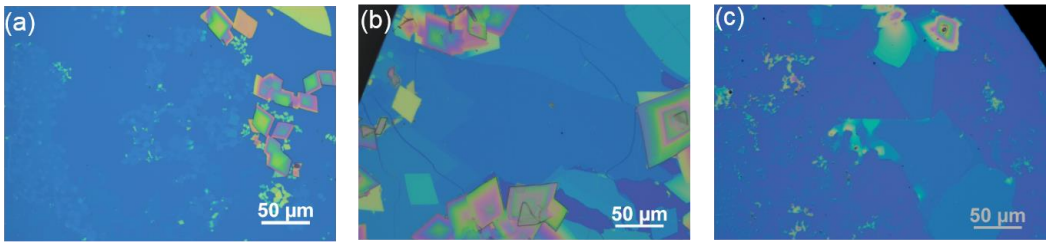

Figure S3. (a-c) Optical microscopy images of C_{10}-DNTT crystals grown at different temperatures.

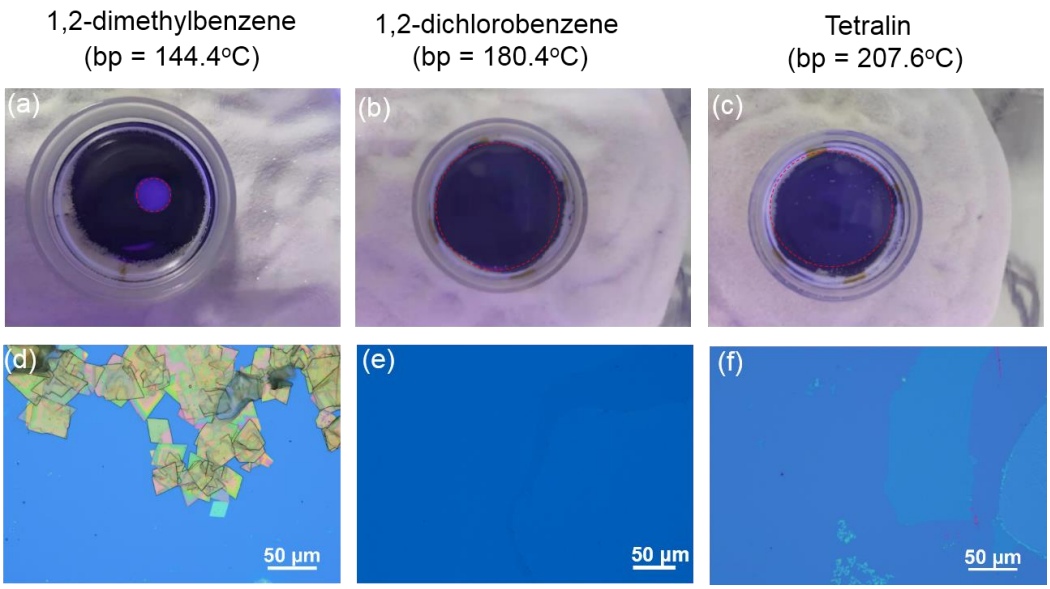

Figure S4. (a-c) Spreading of three types solvents on glycerol at an elevated temperature of 75°C. (a) 1,2-dimethylbenzene, (b) 1,2-dichlorobenzene, and (c) Tetralin. (d-f) Optical microscopy images of C_{10}-DNTT crystals grown in the three types of solvents at an elevated temperature of 75°C. (d) 1,2-dimethylbenzene, (e) 1,2-dichlorobenzene, and (f) Tetralin.

To further elucidate the impacting factors on crystals growth, more types solvents, including 1,2-dimethylbenzene (bp = 144.4°C) and tetralin (bp = 207.6°C), were investigated together with 1,2-dichlorobenzene (Figure S4). All these solvents exhibited high boiling point. As can be seen from Figure S4a-c, their spreading on glycerol surface was different. 1,2-dimethylbenzene solution formed a compact lens, while 1,2-dichlorobenzene and tetralin solution spread well (Figure S4a-c). Combing the produced crystals, it was clear that bad spreading led to small and thick crystals (Figure S4d) while good spreading resulted in large 2DMCs (Figure S4e-f). The different spreading properties of the solvents were determined by their surface tensions (*J. Am. Chem. Soc.* **2018**, *140*, 5339). Judging from the above results, the spreading of the solvent on the liquid substrate affected crystal growth.

Combing the results of Figure 2 and Figure S4, the key factors impacting the production of 2DMCs were (i) the types of the liquid substrate, (ii) the growth temperature, (iii) the boiling point of the solvent, and (iv) the spreading of the solvent on the liquid substrate.

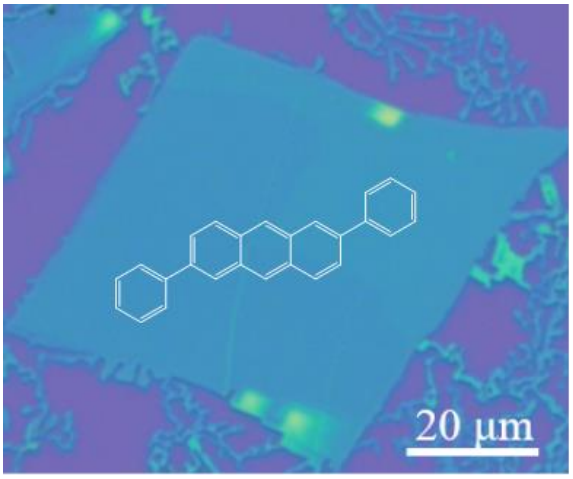

Figure S5. An OM image of 2DMCs of DPA on SiO_2/Si substrate grown by the same method. The solvent was 1,2-dichlorobenzene and the growth temperature was 75°C.

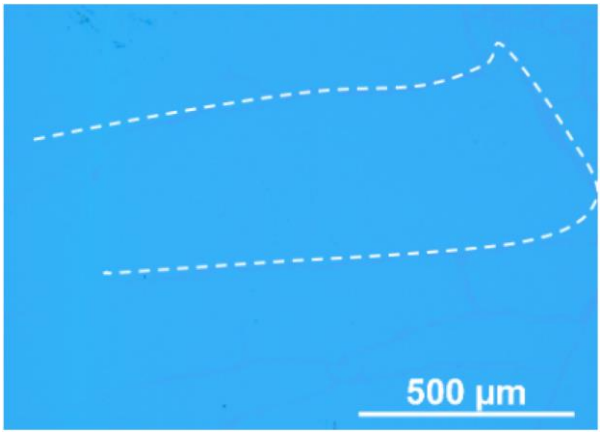

Figure S6. An OM image of a millimeter scale 2DMC of C_{10}-DNTT transferred on SiO_2/Si substrate.

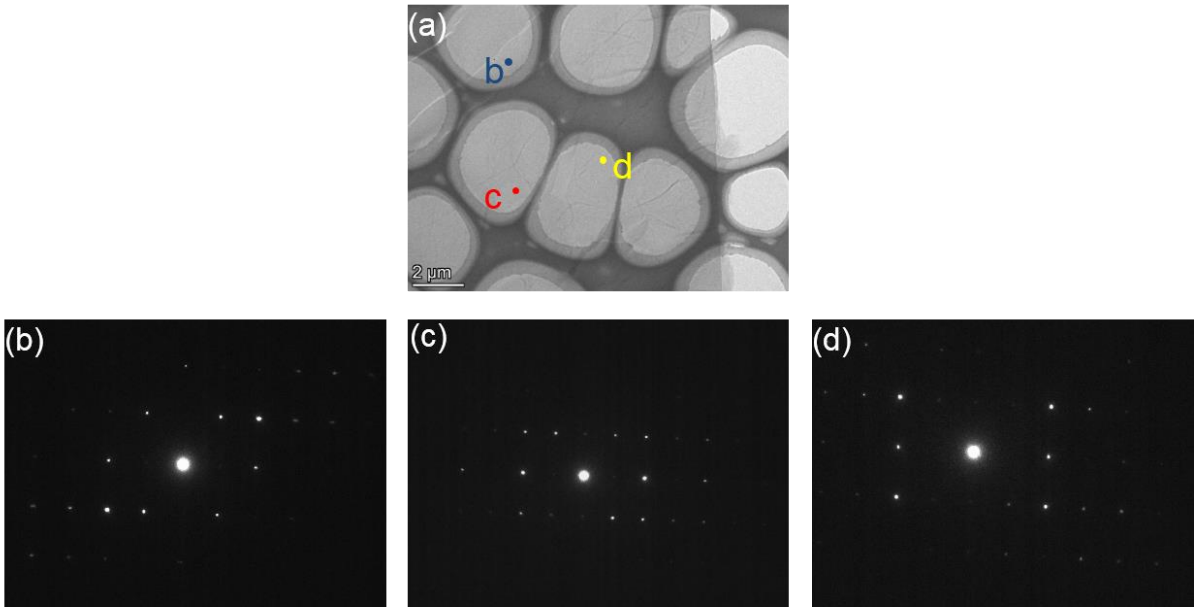

Figure S7. a) TEM of an individual 2DMC and (b–d) the corresponding SAED. The identical SAED patterns at different positions of the 2DMC confirmed its single crystalline nature.

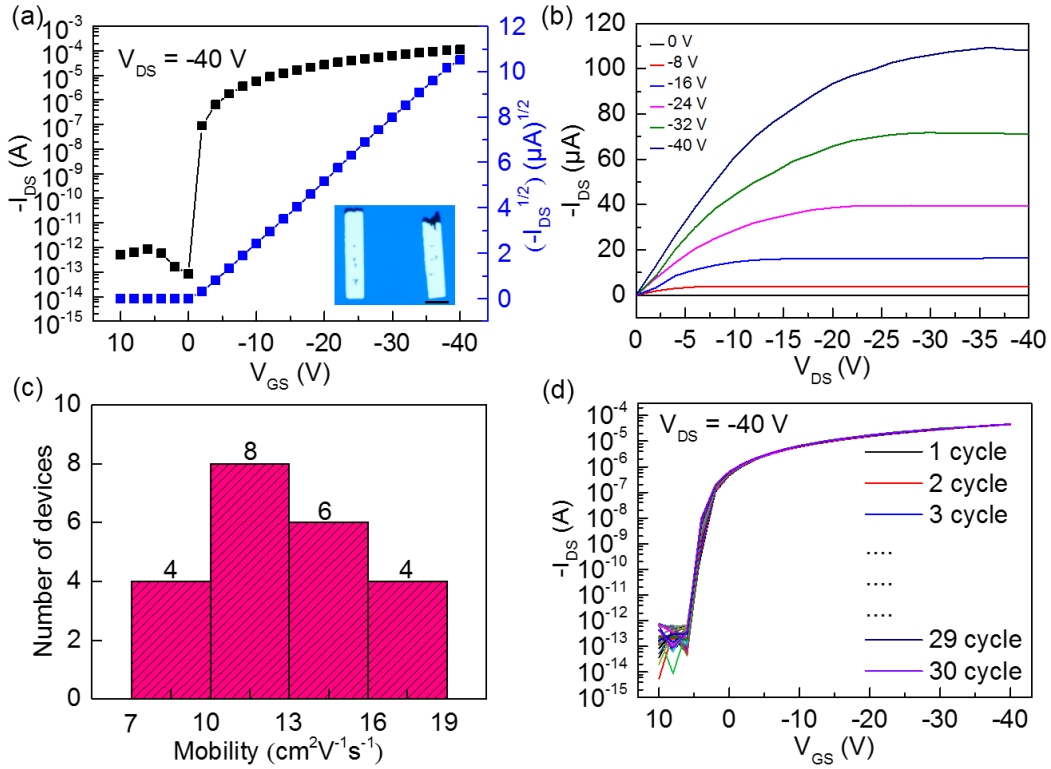

Figure S8. (a) Typical transfer curves of 2DMCs of C_{10}-DNTT, the inset showed a top view OM of the channel area of C_{10}-DNTT (W/L = 1.42). The scale bar is 50 μm. (b) Output curves of 2DMCs of C_{10}-DNTT at different gate voltages. (c) The mobility distribution of 22

devices. (d) Transfer curves of the 2DMC of C_{10}-DNTT under negative gate stress.

The mobility of the OFETs was calculated from the following equation: $I_{DS} = (W/2L)\mu C_i(V_{GS} - V_{th})^2$, where I_{DS} is the source-drain current, μ is the field effect mobility, V_{th} is the threshold voltage, V_{GS} is the applied gate voltage, L is the channel length, W is the channel width and the C_i is the specific capacitance (10 nF cm^{-2}). The maximum mobility (average mobility among 22 devices) was 18.0 (12.2) $cm^2\ V^{-1}\ s^{-1}$.

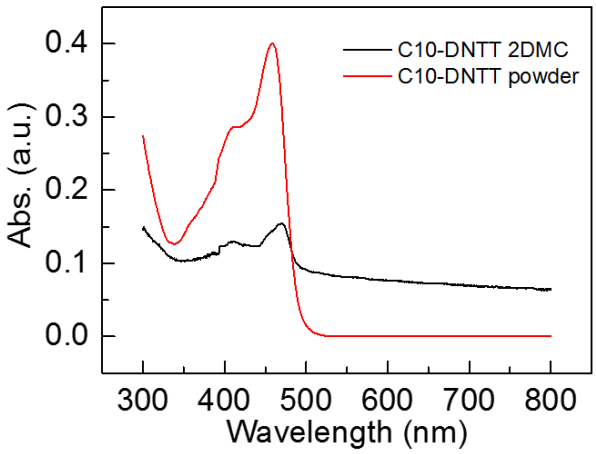

Figure S9. UV-Vis spectra of 2DMCs and powders of C_{10}-DNTT.

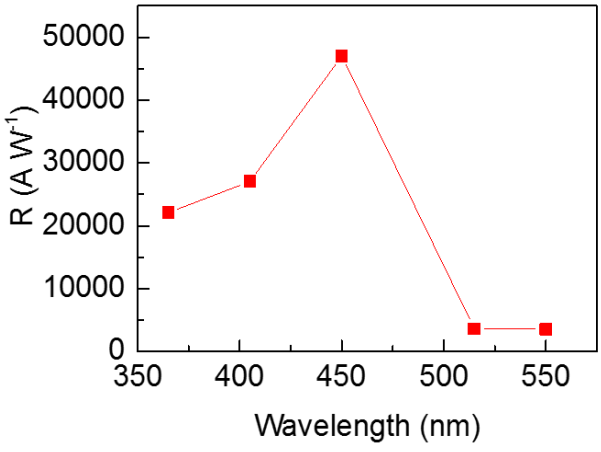

Figure S10. Wavelength dependent photoresponse of 2DMCs of C_{10}-DNTT. The photoresponsivity (Figure S10) agreed well with the absorption (Figure S9).

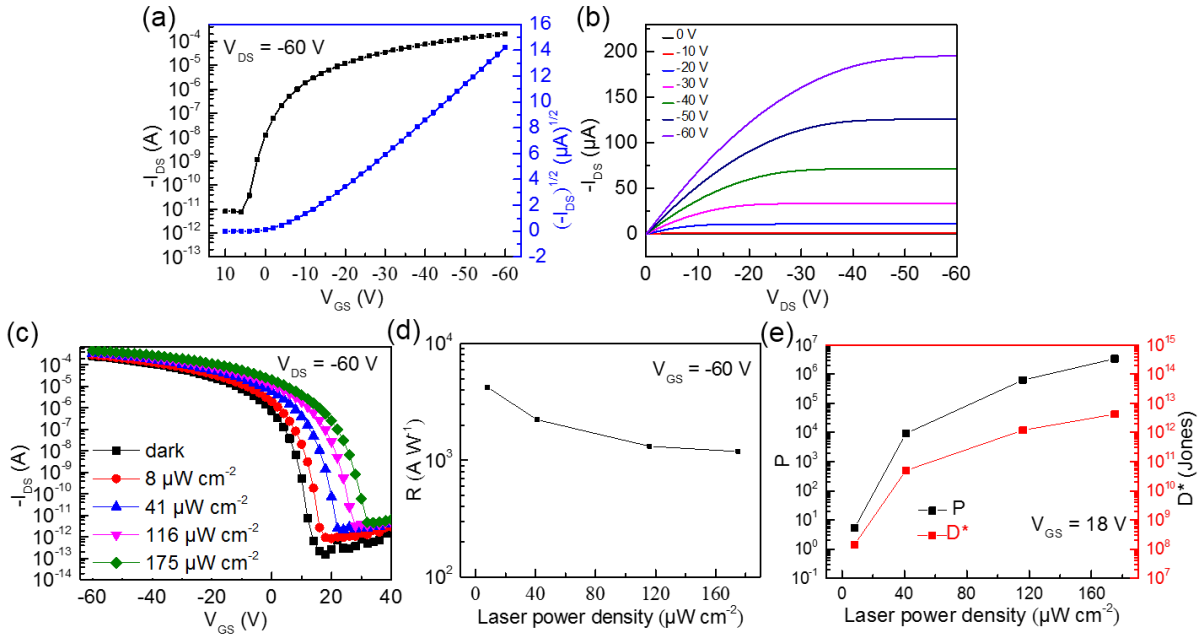

Figure S11. (a) Typical transfer curves of polycrystalline thin films of C_{10}-DNTT (10nm) by vacuum deposition. (b) Output curves of polycrystalline thin films of C_{10}-DNTT at different gate voltages. (c) Ttransfer curves of an OPT based on polycrystalline thin films of C_{10}-DNTT under dark and at different laser power densities. (d) Responsivity as a function of laser power densities (e) Photosensitivity and specific detectivity as a function of laser power densities.

We performed electrical characterization of the vacuum-deposited C_{10}-DNTT polycrystalline film (10 nm), and found that the maximum mobility was 5.9 $cm^2\ V^{-1}\ s^{-1}$ (Figure S11a and Figure S11b). The mobility was much smaller than the 2DMCs of C_{10}-DNTT grown on a liquid substrate at an elevated temperature (maximum mobility of 18.0 $cm^2\ V^{-1}\ s^{-1}$). OPTs based on polycrystalline thin films of C_{10}-DNTT showed inferior photoresponse compared with those based on 2DMCs, with maximum *R*, *P*, and *D** of 4.2 × 10^3 A W^{-1}, 3.4 × 10^6, and 4.3 × 10^{12} Jones, respectively (Figure S11c-e). The enhanced photoresponse of 2DMC-based OPTs could be ascribed to the high carrier mobility of the single crystalline structure of 2DMCs.

Table S1 Summary of phototransistors based on polycrystalline films

Semiconductor	Method	Thickness (nm)	Mobility ($cm^2V^{-1}s^{-1}$)	P	R (A W^{-1})	D* (Jones)	Year	Ref.
Pentacene	vacuum evaporation	100	0.49	10^5	50	N/A	2005	[1]
6T	vacuum evaporation	50–100	0.09	1.3×10^3	1.5~2.4	N/A	2006	[2]
ABT	vacuum evaporation	50	0.4	10^3	800	N/A	2009	[3]
$F_{16}CuPc$	vacuum evaporation	50	5.3×10^{-4}	22	1.5×10^{-3}	N/A	2009	[4]
P3HT	drop-casting	80	0.01-0.07	3.8×10^3	250	N/A	2010	[5]
TIPS-Pentacene	ink-jet printing	50	0.02	10^6–10^7	N/A	N/A	2010	[6]
DPA	vacuum evaporation	20	12	8.5×10^7	1.34×10^5	1.2×10^{17}	2019	[7]

Table S2 Summary of phototransistors based on organic single crystals

Semiconductor	Mobility ($cm^2V^{-1}s^{-1}$)	P	EQE (%)	R (A W^{-1})	D* (Jones)	Year	Ref.
Me-ABT	1.66	2×10^4	N/A	5×10^4	N/A	2010	[8]
A-EHDTT	1.2-1.6	1.4×10^5	N/A	1.4×10^4	N/A	2011	[9]
PY-4(THB)	0.7	1.2×10^6	N/A	2×10^3	N/A	2011	[10]
BBDTE	1.62	10^5	N/A	9.8×10^3	N/A	2015	[11]
p-DTS($FBTTh_2$)$_2$	1.8	10^3–10^4	N/A	3×10^3	N/A	2018	[12]
TFT-CN	1.36	5×10^5	4×10^6	9×10^4	6×10^{14}	2018	[13]
TIPS-Pentacene	2.06	1.36×10^8	2.9×10^5	845	1.98×10^{15}	2019	[14]
C6-DPA	1.81	8.8×10^7	N/A	2.63×10^2	6.7×10^{14}	2019	[15]
1,6-DTEP	2.1	1.60×10^5	N/A	2.86×10^6	1.49×10^{18}	2020	[16]
2,7-DTEP	2.1	4.35×10^3	N/A	1.04×10^5	5.28×10^{16}	2020	[16]
C_{10}-DNTT	18	1.7×10^7	3.2×10^7	4.7×10^4	2.6×10^{16}	2020	This work

Table S3 Boiling points of the liquids used in this study

liquid	water	glycerol	methylbenzene	Chlorobenzene	1,2-dichlorobenzene
Temperature (^oC)	100	290.9	110.6	132.2	180.4

Reference

1. Y.-Y. Noh, D.-Y. Kim and K. Yase, *J. Appl. Phys.*, 2005, **98**, 074505.
2. Y.-Y. Noh, J. Ghim, S.-J. Kang, K.-J. Baeg, D.-Y. Kim and K. Yase, *J. Appl. Phys.*, 2006, **100**, 094501.
3. Y. Guo, C. Du, C.-a. Di, J. Zheng, X. Sun, Y. Wen, L. Zhang, W. Wu, G. Yu and Y. Liu, *Appl. Phys. Lett.*, 2009, **94**, 143303.

4. B. Mukherjee, M. Mukherjee, Y. Choi and S. Pyo, *J. Phys. Chem. C*, 2009, **113**, 18870.
5. T. Pal, M. Arif and S. I. Khondaker, *Nanotechnology*, 2010, **21**, 325201.
6. Y.-H. Kim, J.-I. Han, M.-K. Han, J. E. Anthony, J. Park and S. K. Park, *Org. Electron.*, 2010, **11**, 1529.
7. D. Ji, T. Li, J. Liu, S. Amirjalayer, M. Zhong, Z.-Y. Zhang, X. Huang, Z. Wei, H. Dong, W. Hu and H. Fuchs, *Nat. Commun.*, 2019, **10**, 12.
8. Y. Guo, C. Du, G. Yu, C.-a. Di, S. Jiang, H. Xi, J. Zheng, S. Yan, C. Yu, W. Hu and Y. Liu, *Adv. Funct. Mater.*, 2010, **20**, 1019.
9. K. H. Kim, S. Y. Bae, Y. S. Kim, J. A. Hur, M. H. Hoang, T. W. Lee, M. J. Cho, Y. Kim, M. Kim, J. I. Jin, S. J. Kim, K. Lee, S. J. Lee and D. H. Choi, *Adv. Mater.*, 2011, **23**, 3095.
10. Y. S. Kim, S. Y. Bae, K. H. Kim, T. W. Lee, J. A. Hur, M. H. Hoang, M. J. Cho, S. J. Kim, Y. Kim, M. Kim, K. Lee, S. J. Lee and D. H. Choi, *Chem. Commun.*, 2011, **47**, 8907.
11. G. Zhao, J. Liu, Q. Meng, D. Ji, X. Zhang, Y. Zou, Y. Zhen, H. Dong and W. Hu, *Adv. Electron. Mater.*, 2015, **1**, 1500071.
12. Q. Cui, Y. Hu, C. Zhou, F. Teng, J. Huang, A. Zhugayevych, S. Tretiak, T.-Q. Nguyen and G. C. Bazan, *Adv. Funct. Mater.*, 2018, **28**, 1702073.
13. C. Wang, X. Ren, C. Xu, B. Fu, R. Wang, X. Zhang, R. Li, H. Li, H. Dong, Y. Zhen, S. Lei, L. Jiang and W. Hu, *Adv. Mater.*, 2018, **30**, e1706260.
14. Y. Zhang, X. Zhu, S. Yang, F. Zhai, F. Zhang, Z. Niu, Y. Feng, W. Feng, X. Zhang, L. Li, R. Li and W. Hu, *Nanoscale*, 2019, **11**, 12781.
15. J. Y. Yao, Y. Z. Zhang, X. T. Tian, X. Z. Zhang, H. Z. Zhao, X. Z. Zhang, J. J. Jie, X. W. Wang, R. L. Li and W. Hu, *Angew. Chem., Int. Ed.*, 2019, **58**, 16082.
16. J. Tao, D. Liu, Z. Qin, B. Shao, J. Jing, H. Li, H. Dong, B. Xu and W. Tian, *Adv. Mater.*, 2020, **32**, e1907791.